

XMM-Newton observations of the extremely X-ray luminous quasar CFHQS J142952+544717=SRGE J142952.1+544716 at redshift $z=6.18$

Medvedev P.¹ *, Gilfanov M.^{1,2}, Sazonov S.^{1,3}, Schartel N.⁴, Sunyaev R.^{1,2}

¹*Space Research Institute (IKI), Russian Academy of Sciences, Profsoyuznaya ul. 84/32, Moscow, 117997 Russia*

²*Max-Planck-Institut für Astrophysik (MPA), Karl-Schwarzschild-Str. 1, D-85741 Garching, Germany*

³*Moscow Institute of Physics and Technology, Institutsky per. 9, 141700 Dolgoprudny, Russia*

⁴*European Space Agency (ESA), European Space Astronomy Centre (ESAC), E-28691 Villanueva de la Cañada, Madrid, Spain*

Last updated ...; in original form ...

ABSTRACT

We present results from a 20 ks *XMM-Newton* DDT observation of the radio-loud quasar CFHQS J142952+544717 at $z = 6.18$, whose extreme X-ray luminosity was recently revealed by the *SRG/eROSITA* telescope in the course of its first all-sky survey. The quasar has been confidently detected with a total of ~ 1400 net counts in the 0.2–10 keV energy band (1.4 to 72 keV in the object’s rest frame). Its measured spectrum is unusually soft and can be described by an absorbed power-law model with a photon index of $\Gamma = 2.5 \pm 0.2$. There are no signs of a high-energy cutoff or reflected component, with an 90 per cent upper limit on the fluorescence iron $K\alpha$ equivalent width of ≈ 290 eV and the corresponding upper limit on the iron K-edge absorption depth of 0.6. We have detected, at the > 95 per cent confidence level, an excess absorption above the Galactic value, corresponding to a column density $N_H = 3 \pm 2 \times 10^{22} \text{ cm}^{-2}$ of material located at $z = 6.18$. The intrinsic luminosity of CFHQS J142952+544717 in the 1.4 to 72 keV energy band is found to be $5.5^{+0.8}_{-0.6} \times 10^{46} \text{ erg s}^{-1}$. We did not detect statistically significant flux changes between two *SRG* scans and the *XMM-Newton* observation, spanning over ~ 7.5 months, implying that the quasar remained at this extremely high luminosity level for at least a month in its rest frame. We put forward the hypothesis that the extreme X-ray properties of CFHQS J142952+544717 are associated with inverse Compton scattering of cosmic microwave background photons (at $z = 6.18$) in its relativistic jets.

Key words: galaxies: active, galaxies: high-redshift, galaxies: nuclei, X-rays: general, individual: CFHQS J142952+544717

1 INTRODUCTION

CFHQS J142952+544717 is a radio-loud, optically luminous distant quasar at a redshift of 6.18. CFHQS J142952+544717 belongs to the bright end of the quasar luminosity function at $z \sim 6$ (e.g. Willott et al. 2010), but is not extremely bright, being ~ 1.5 magnitudes fainter than the most optically luminous quasars known at these redshifts. With a radio-loudness parameter of $R \sim 100$, the quasar has a steep radio spectrum with no significant variability detected in the radio (for detailed discussion, see Medvedev et al. 2020). According to these properties, relativistic beaming is unlikely to play a major role in the appearance of the source, and therefore CFHQS J142952+544717 is unlikely to be a blazar.

Recently, Medvedev et al. (2020) have discovered an X-ray signal from CFHQS J142952+544717 by cross-matching the catalogue of sources detected in the first *SRG/eROSITA* all-sky survey with the Pan-STARRS1 (PS1) distant quasar sample in the redshift range of $5.6 < z < 6.7$ (Bañados et al. 2016). With the measured luminosity of $2.6^{+1.7}_{-1.0} \times 10^{46} \text{ erg s}^{-1}$ in the rest-frame 2–10 keV energy band, the object (called SRGE J142952.1+544716 in the *SRG/eROSITA* catalogue) turned out to be the most X-ray luminous quasar known at

$z > 6$ ¹. Because of the small number (~ 10) of photons detected by *eROSITA*, only a crude spectral analysis was done by Medvedev et al. (2020), which provided loose constraints on the power-law photon index: $\Gamma = 1.4 \pm 0.9$.

Following the discovery of the extreme X-ray luminosity of this quasar, an *XMM-Newton* (Jansen et al. 2001) Director’s Discretionary Time (DDT) observation of CFHQS J142952+544717 was scheduled in the summer 2020, aimed at obtaining a high-quality X-ray spectrum of the source and investigating its short- and long-term scale variability. The results of these *XMM-Newton* observations as well as from the second scan of this source by *SRG/eROSITA* during its ongoing all-sky survey are reported below.

In what follows, we adopt a flat Λ CDM cosmological model with $h = 0.70$ and $\Omega_\Lambda = 0.7$, and the quasar’s redshift $z = 6.183$ (Wang et al. 2011).

2 DATA REDUCTION AND METHODS

CFHQS J142952+544717 was observed with *XMM-Newton* on 2020 July 24 for 23 ks of Director’s Discretionary Time (revolution 3777,

¹ A second quasar with comparably high X-ray luminosity was recently discovered by *SRG/eROSITA* at a slightly smaller redshift of $z = 5.47$ (?)

* Contact e-mail: tomedvedev@iki.rssi.ru

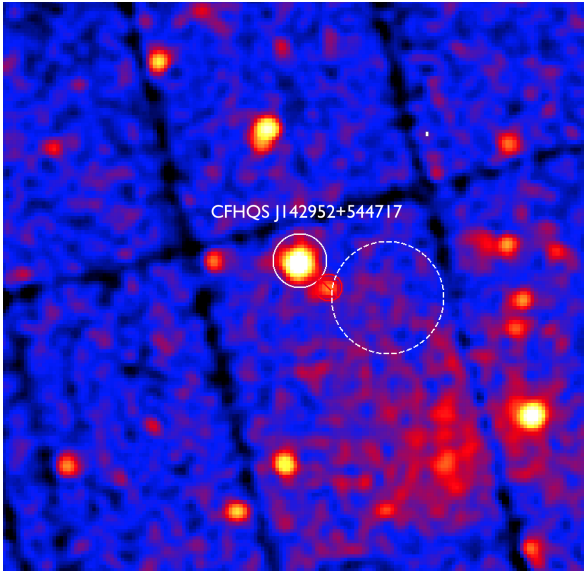


Figure 1. Mosaic image of CFHQS J142952+544717 = SRGE J142952.1+544716 obtained by *XMM-Newton*, including all three EPIC cameras, in the 0.2–12 keV band, smoothed with a Gaussian filter with $\sigma = 1.5$. The white circles show extraction regions for the PN spectra: the solid circle of 30 arcsec radius is the source region and the dashed circle of ≈ 60 arcsec radius is the background region. The red circle (12 arcsec) masks a faint source and was excluded from the background extraction region.

obsID 0871191201). The European Photon Imaging Camera (EPIC, [Strüder et al. 2001](#); [Turner et al. 2001](#)) was operated in full-frame mode with thin filters. The event lists for the EPIC cameras were obtained from the processed pipeline products (PPS) retrieved from the *XMM-Newton* Science Archive. As a first step, we selected all events that were not affected by proton flares. The total cleaned exposure times are 19.7 and 21 ks for the PN and MOS cameras, respectively.

We extracted the source spectra using a circle region with a radius of 30 arcsec centred on the best-fitting source position from the maximum-likelihood source list (ML-list) for PSF fitting provided by PPS. For the background extraction, we used a 60 arcsec circle avoiding CCD gaps for PN (see Fig. 1) and 3 circles (of 100, 90, and 70 arcsec) in a source free area for the MOS cameras. For each spectrum we generated the response matrix and the ancillary file using the Science Analysis System (SAS v.18.0.0) tasks RMFGEN and ARFGEN. Event patterns 0–12 were included for the MOS cameras, while for the PN camera we used patterns 0–4. The net source count rates obtained are $1.0 \pm 0.1 \times 10^{-2}$, $1.0 \pm 0.1 \times 10^{-2}$ and $4.6 \pm 0.2 \times 10^{-2}$ cts s^{-1} for MOS-1, MOS-2 and PN, respectively. We did not consider the RGS data, since the source is too faint ($\ll 0.1$ cts s^{-1}) for a meaningful RGS spectral analysis.

The spectra were rebinned to ensure a minimum of 5 counts per energy bin by means of the standard tool GRPPHA. Then we use the C-statistic ([Cash 1979](#)) modified to account for the Poisson background subtraction (the ‘W-statistic’ in XSPEC, version 12.11.0, [Arnaud 1996](#)) to analyse the data. Once the best-fitting model is obtained, we run a Monte Carlo Markov Chain (MCMC) within XSPEC, using the Goodman-Weare algorithm ([Goodman & Weare 2010](#)) with 10^5 steps to explore the parameter space. All subsequent errors are calculated using MCMC chains and quoted at the 90 per cent confidence level. We also examine the goodness-of-fit for individual models by using the ‘goodness’ command in XSPEC with

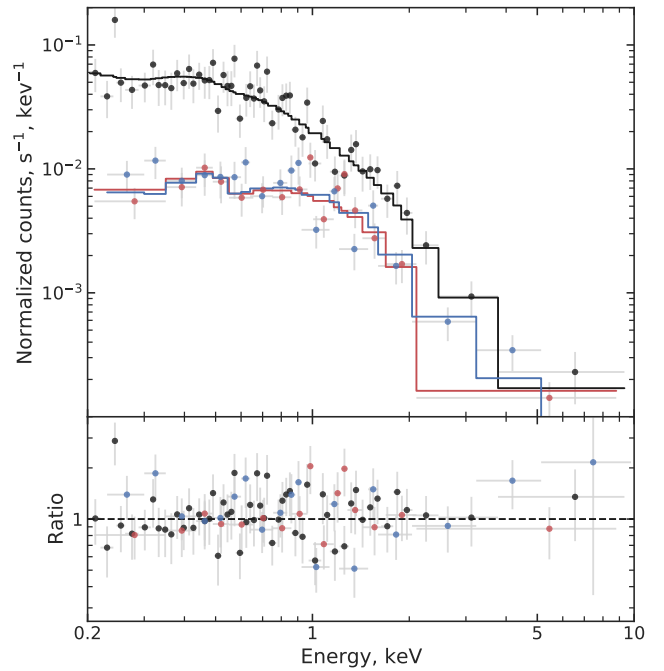


Figure 2. EPIC-PN (black) and EPIC-MOS (red and blue) spectra of CFHQS J142952+544717. The spectral bins are combined to have a significant detection of at least 3σ (for plotting purposes only). The solid lines show an absorbed power-law model providing the best simultaneous fit to the data in the 0.2–10 keV range (see model 1 in Table 1). The bottom panel shows the ratio of the data to the folded model. The shown observed energy range corresponds to the 1.4–72 keV range in the quasar’s rest frame.

Anderson-Darling (AD) test statistic (see, e.g., Appendix B in the XSPEC manual for definition). This test reports the fraction of simulations having an AD statistic smaller than that for the observed spectrum. In what follows, we run this command with ‘nosim’ and ‘fit’ options, which means that all simulations are drawn from the best-fitting model; then each simulated data set is fitted to the model and new test statistic is calculated (also referred to as the parametric bootstrap method, see, e.g. [Feigelson & Babu 2012](#)). For the ‘goodness’ test, we run 100,000 realisations for each model. As is well known, the goodness-of-fit test result should not be interpreted as the probability of the model being (in)correct, rather it helps spot those models whose best-fitting statistic values are too high to be a result of a statistical fluctuation.

3 RESULTS

CFHQS J142952+544717 is clearly detected in the *XMM-Newton* EPIC images (see Fig. 1), with ≈ 1400 net counts from the source in the 0.2–12 keV energy range. The spectrum is relatively soft, but the source is nevertheless confidently detected in the 4.5–7.5 keV band. In this energy range, we detected a total of 72 counts in the source extraction region, with the expected background contribution of 52.9 counts (the Poisson probability is $\ln(p) = -5.3$, corresponding to $\approx 2.8\sigma$ for Gaussian distribution). No detection was obtained in the 7.5–12 keV band at 90 per cent confidence; given a total of 69 registered counts with the expected background contribution of 61.2 counts ($\ln(p) = -1.9$), the corresponding upper limit flux is 5.5×10^{-14} erg cm^{-2} s^{-1} .

Since the *XMM-Newton* astrometric accuracy from the attitude solutions is subject to systematic uncertainties, typically ~ 1 arcsec (e.g., Gabriel et al. 2017), the cross-match of the EPIC sources from the ML-list with sources from DSS-DR9 is performed during the pipeline data processing. In the case of the CFHQS J142952+544717 observation, we found offsets in the RA, DEC position of 0.97 and -1.47 arcsec, respectively. The corrected X-ray source position is $\alpha = 14^h 29^m 52.188^s$, $\delta = +54^d 47^m 17.86^s$ with the statistical error RADEC_ERR = 0.25 arcsec and the error arising from the field rectification SYSERRRCC = 0.39 arcsec, which combined can be translated to a 1σ positional uncertainty of 0.5 arcsec. The obtained position is 0.5 arcsec offset from the optical position of the quasar CFHQS J142952+544717 ($\alpha = 14^h 29^m 52.146^s$, $\delta = +54^d 47^m 17.55^s$) in CFHTLS (Hudelot et al. 2012), while the nearby serendipitous source CFHT 1323_175499 discussed in Medvedev et al. (2020) is 2.1 arcsec away from the X-ray source. We thus confirm the conclusion drawn in Medvedev et al. (2020) that the X-ray source SRGEJ142952.1+544716 is indeed associated with the quasar CFHQS J142952+544717.

On the *XMM-Newton* image (Fig. 1), there is a weak X-ray source located at $\alpha = 14^h 29^m 48.246^s$, $\delta = +54^d 46^m 50.28^s$, $\approx 40''$ to the south-west of CFHQS J142952+544717. This source has a counterpart in SDSS with $z = 21.09 \pm 0.44$ mag, $i = 21.95 \pm 0.25$ mag (shown by the red circle). Its optical colours suggest that it is a relatively nearby object and is therefore unrelated to CFHQS J142952+544717.

3.1 X-ray spectrum

The ~ 1400 net counts detected from the source enable its detailed spectral analysis. We fitted the individual EPIC camera spectra simultaneously in the 0.2–10 keV energy range, adding cross-normalization factors between the cameras and allowing them to vary. The results of the spectral fitting are summarized in Table 1.

We started by fitting the data with an absorbed power-law model. We first fixed the neutral hydrogen column density at the Galactic value in the direction of CFHQS J142952+544717, $N_H = 1.15 \times 10^{20} \text{ cm}^{-2}$ (HI4PI Collaboration et al. 2016) and obtained an inadequate fit with the cstat value of 279 for 260 d.o.f and the goodness of the fit value of 99 per cent. We therefore thawed the absorption and repeated the fit again. The folded EPIC spectra along with the best-fitting model are shown in Fig. 2, the best-fitting parameters are summarized in Table 1. We obtained a fairly soft power-law spectrum with a photon index of $\Gamma = 2.5 \pm 0.2$ and an absorption column density of $N_H = 4 \pm 2 \times 10^{20} \text{ cm}^{-2}$. The Galactic absorption column is thus outside of the error interval at more than 90 per cent confidence. To examine the quality of the fit, we ran a ‘goodness’ simulation (see Section 2). It showed that 74 per cent of the realisations have the value of AD statistic smaller than that obtained for the real data, suggesting that the model provides an acceptable fit to the observed spectrum.

Using the best-fitting model, we find that the X-ray luminosity of CFHQS J142952+544717 is $L_X = 3.0^{+0.6}_{-0.4} \times 10^{46} \text{ erg s}^{-1}$ in the rest-frame 2–10 keV energy band, in good agreement with the previous measurement by *SRG/eROSITA* (Medvedev et al. 2020). The luminosity in the entire observed energy range (1.4–72 keV in the rest frame) is $5.5^{+0.8}_{-0.6} \times 10^{46} \text{ erg s}^{-1}$.

As a next step, we searched for evidence of a high-energy roll-over in the spectrum. To this end, we replaced the power-law component by the ZCUTOFFPL model in XSPEC with the redshift fixed at 6.183 and the absorption column density fixed at the Galactic value. We found no significant evidence for continuum curvature at the high-energy end of the spectrum with a 90 per cent lower limit on the e -folding

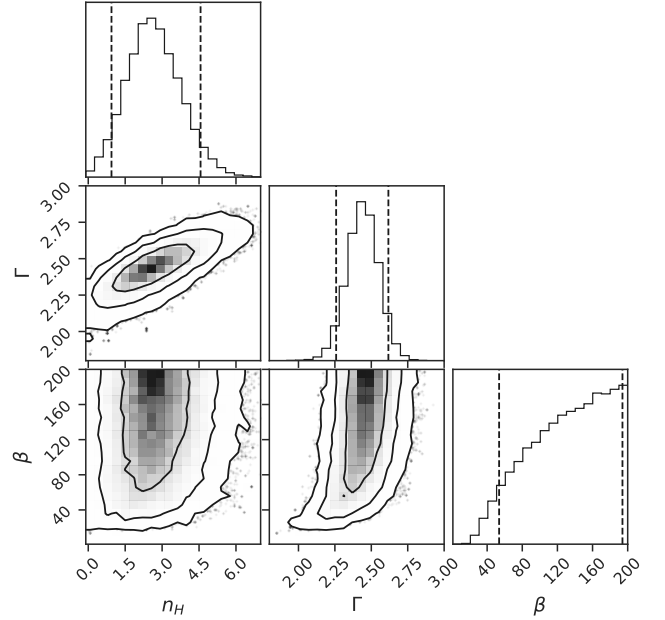


Figure 3. One- and two-dimensional projections of the posterior probability distributions over 3 parameters of model 3 (see Table 1): intrinsic column density (10^{22} cm^{-2}), power-law photon index and high-energy cut-off (rest frame, keV). Contours represent the 68, 95 and 99.7 per cent probability regions, sample points outside of these regions being plotted as gray dots. The vertical dashed lines show the 0.05 and 0.95 quantiles (90 per cent confidence).

energy of the exponential cut-off of $\beta = 29 \text{ keV}$ ($\approx 4 \text{ keV}$ in the observer’s frame). As no extra absorption was included in the model, the fitting resulted in a flatter photon index of $\Gamma = 2.2^{+0.1}_{-0.2}$. The model gives a slightly worse fit statistics, by ΔC -statistic = 6 for the same value of $d.o.f = 259$, confirming a preference for some additional absorption by the data. Running a ‘goodness’ test, we found that 97 per cent of the realisations have a lower AD statistic.

We further added an intrinsic absorption by material located at $z = 6.183$ to the absorbed cutoff power-law model. The posterior probability distributions and confidence contours for the photon index Γ , intrinsic neutral hydrogen column N_H and cutoff energy β are shown in Fig. 3. Comparing the Akaike Information criterion (Akaike 1974) for this model with that for model 1 (see Table 1), we can again confirm that the high energy cut-off is not required by the data, the model with the cutoff yielding almost the same best-fitting statistics but with an increased number of free parameters. In contrast, the intrinsic absorption in excess of the Galactic value is detectable with more than 95 per cent confidence, with the best-fitting value of $N_H = 3 \pm 2 \times 10^{22} \text{ cm}^{-2}$.

Finally, we searched for signs of a reflection component, namely, the iron $K\alpha$ fluorescent emission line and the corresponding absorption edge. To this end, we added to the absorbed power-law model a narrow line ($\sigma = 10 \text{ eV}$) centred at 6.4 keV and an absorption edge at 7.1 keV in the quasar’s rest frame. We found no evidence for an iron line with a 90 per cent upper limit on its equivalent width of 40 eV in the observer’s frame, which translates to $\approx 290 \text{ eV}$ in the quasar’s rest frame. For the depth of the absorption edge, we obtained a non-zero best-fitting value of $\tau_{\text{edge}} = 0.3^{+0.3}_{-0.2}$, which, however, is consistent with zero at the ~ 95 per cent confidence level, see Fig. 4.

Table 1. Results of the spectral analysis for the *XMM-Newton* observation of CFHQS J142952+544717. In all models, the redshift is fixed at 6.183 if applicable. The abundance set by [Wilms et al. \(2000\)](#) is used in all absorption models. The quoted broad-band (0.2–10 keV) flux is the flux for the best-fitting model to PN-data corrected for the Galactic and intrinsic absorption. N_{M1} and N_{M2} stand for the MOS1-to-PN and MOS2-to-PN cross-calibration factors, respectively. The cstat values correspond to the negative of twice the logarithm of the likelihood of the model (by definition). The ‘goodness’ values, below the AD statistic values, denote the percentage of realisations of the model that have a lower AD statistic than the data (obtained by the ‘goodness’ command in XSPEC). Thus, larger ‘goodness’ values indicate a smaller probability of obtaining such a poor fit by chance. The Akaike information criterion (AIC) is calculated as $AIC = 2k + cstat$, where k is the number of free parameters in the fit, the preferred model for the data being the one with the minimum AIC.

Xspec Model	Parameters	Parameter Values	cstat/d.o.f	log(AD) (goodness)	AIC
1. CONST*TBABS*POW	N_H	$4 \pm 2 \times 10^{20} \text{ cm}^{-2}$	272/259	-7.48 (73.9%)	281.6
	Γ	2.5 ± 0.2			
	N_{M1}	$1.1^{+0.2}_{-0.1}$			
	N_{M2}	1.2 ± 0.2			
	$F_{0.2-10}$	$1.3^{+0.2}_{-0.1} \times 10^{-13} \text{ erg cm}^{-2} \text{ s}^{-1}$			
2. CONST*TBABS* ZCUTOFFPL	N_H^*	$1.15 \times 10^{20} \text{ cm}^{-2}$	278/259	-6.68 (97.4%)	288.1
	Γ	$2.2^{+0.1}_{-0.2}$			
	β	$> 29 \text{ keV}$			
	N_{M1}	$1.1^{+0.2}_{-0.1}$			
	N_{M2}	1.2 ± 0.2			
	$F_{0.2-10}$	$1.08^{+0.09}_{-0.10} \times 10^{-13} \text{ erg cm}^{-2} \text{ s}^{-1}$			
3. CONST*TBABS* ZPHABS*ZCUTOFFPL	N_H^*	$1.15 \times 10^{20} \text{ cm}^{-2}$	271/258	-7.23 (86.9%)	283.5
	N_H^z	$3 \pm 2 \times 10^{22} \text{ cm}^{-2}$			
	Γ	2.5 ± 0.2			
	β	$> 54 \text{ keV}$			
	N_{M1}	$1.1^{+0.2}_{-0.1}$			
	N_{M2}	1.1 ± 0.2			
	$F_{0.2-10}$	$1.2^{+0.2}_{-0.1} \times 10^{-13} \text{ erg cm}^{-2} \text{ s}^{-1}$			
4. CONST*TBABS* ZPHABS* (ZEDGE*POW + ZGAUSS)	N_H^*	$1.15 \times 10^{20} \text{ cm}^{-2}$	267/257	-7.76 (55.3%)	281.5
	N_H^z	$3 \pm 2 \times 10^{22} \text{ cm}^{-2}$			
	Γ	2.5 ± 0.2			
	τ_{edge}	$0.3^{+0.3}_{-0.2}$			
	$EW_{\text{Fe K}\alpha}$	$< 40 \text{ eV}$			
	$\sigma_{\text{Fe K}\alpha}^*$	10 eV			
	N_{M1}	$1.1^{+0.2}_{-0.1}$			
	N_{M2}	1.1 ± 0.2			
	$F_{0.2-10}$	$1.3^{+0.2}_{-0.1} \times 10^{-13} \text{ erg cm}^{-2} \text{ s}^{-1}$			

* Parameter is fixed during the fit.

We conclude that no spectral features associated with iron absorption and fluorescence have been detected in the data.

3.2 Light curve

Figure 5 shows the EPIC cameras combined, background-subtracted light curve of CFHQS J142952+544717 in the 0.2–8 keV energy range. We did not detect any statistically significant short-term variability, with the Fourier power spectrum being consistent with zero. Overall, the *XMM-Newton* light curve may suggest some increasing trend, however, its statistical significance is low. Indeed, dividing the data into two halves and using model 1 from Table 1, we measure the 0.2–10 keV band flux of $F_{0.2-10} = 1.17^{+0.19}_{-0.15} \times 10^{-13}$ and $F_{0.2-10} = 1.49^{+0.24}_{-0.18} \times 10^{-13} \text{ erg cm}^{-2} \text{ s}^{-1}$ for the first and second half, respectively.

These two values are consistent with each other within 90 per cent confidence. Thus, although the intra-day variability of CFHQS J142952+544717 is an interesting possibility, which might dramatically impact the theoretical models for this source, it cannot be established with the due statistical significance at this stage.

We also checked if CFHQS J142952+544717 is variable on timescales of months by comparing two *eROSITA* measurements conducted during the first and the second *SRG* all-sky surveys with the *XMM-Newton* measurement. The quasar position was scanned by *SRG* on 2019 December 10–11 during eRASS I and on 2020 June 6–9 during eRASS II. Using the best-fitting model 1 from Table 1, we find the absorption uncorrected fluxes $F_{0.2-6}^{\text{eI}} = 1.1^{+0.6}_{-0.5} \times 10^{-13} \text{ ergs cm}^{-2} \text{ s}^{-1}$ and $F_{0.2-6}^{\text{eII}} = 1.3 \pm 0.6 \times 10^{-13} \text{ ergs cm}^{-2} \text{ s}^{-1}$ in the 0.2–6 keV energy range for eRASS I and II, respectively. We note that these flux values are based on pre-flight absolute flux calibrations

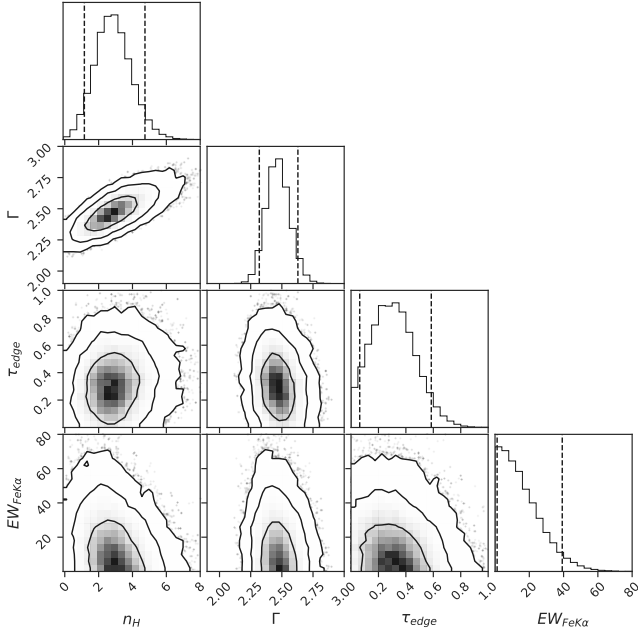


Figure 4. Corner plot over 4 parameters of model 4 (see Table 1): intrinsic column density (10^{22} cm^{-2}), power-law photon index, absorption depth at rest-frame energy 7.1 keV (or 0.99 keV in the observer’s frame) and equivalent width of Fe $K\alpha$ line at rest-frame energy 6.4 keV (or 0.9 keV in the observer’s frame, eV). Contours represent the 68, 95 and 99 per cent probability regions, sample points outside of these regions being plotted as gray dots. The vertical dashed lines show the 0.05 and 0.95 quantiles (90 per cent confidence).

of the *eROSITA* telescope. The given errors are statistical only (90 per cent confidence). The corresponding flux during *XMM-Newton* observation is $F_{0.2-6} = 8.4^{+0.6}_{-0.7} \times 10^{-14} \text{ ergs cm}^{-2} \text{ s}^{-1}$ and is thus consistent, within statistical and systematic uncertainties, with the *eROSITA* measurements taken ~ 7 and ~ 1.5 months earlier.

We conclude that no statistically significant variability of the source has been detected.

4 DISCUSSION

The *XMM-Newton* observations have confirmed beyond any doubt the association of the X-ray source SRGEJ142952.1+544716 discovered by *SRG/eROSITA* with the quasar CFHQS J142952+544717 at $z = 6.18$. The flux measurements taken with *eROSITA* and *XMM-Newton* at three epochs between Dec. 2019 and July 2020 indicate that the X-ray luminosity of CFHQS J142952+544717 remained at an extremely high and nearly constant level for at least a month in the quasar’s rest frame.

The X-ray spectrum measured with *XMM-Newton* in the rest-frame 1.4–72 keV energy band has a simple power-law shape (slightly modified by absorption at low energies) without any significant features (Fig. 6). The steep slope of $\Gamma_x = 2.5 \pm 0.2$ is unusual for both Seyfert galaxies (e.g. Malizia et al. 2014; Ricci et al. 2017) and quasars (e.g. Shemmer et al. 2008), including those at $z \sim 6$ (Nanni et al. 2017), with the vast majority of the well-studied active galactic nuclei (AGN) having X-ray continua characterised by $\Gamma \sim 1.5\text{--}2.2$, usually interpreted in terms of Comptonization of accretion disc emission in a hot corona.

The overall spectral energy distribution (SED) of

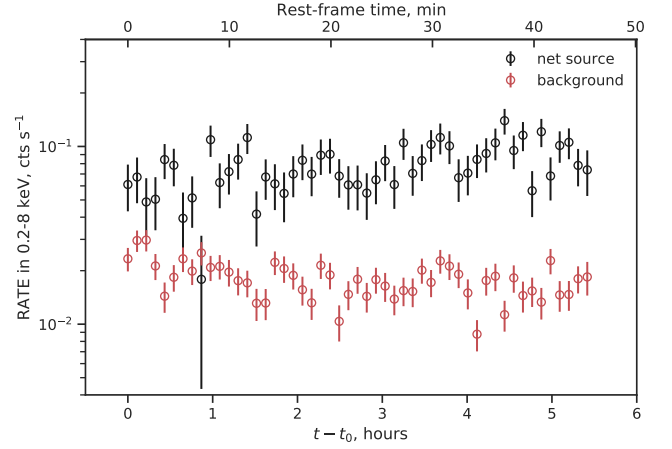


Figure 5. Combined EPIC-PN and -MOS light curves of CFHQS J142952+544717 in the 0.2–8 keV energy ranges. The horizontal axis shows time since the start of the observation on 2020-07-24 12:27 UTC (in hours), the time bin is 390 s. The top axis shows time in the quasar’s rest frame (in minutes). The black circles show background subtracted source count rates, while the red circles show background rates.

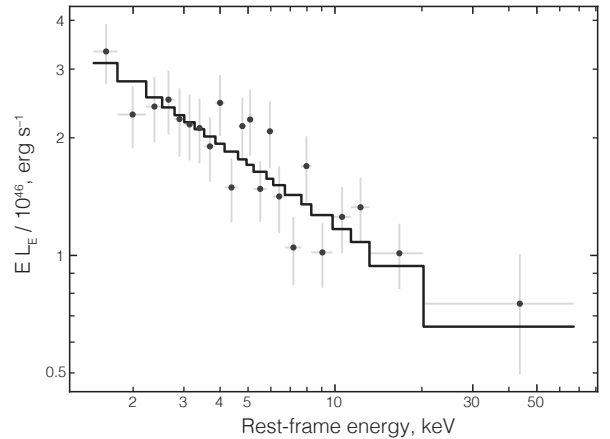


Figure 6. *XMM-Newton* EPIC-PN unfolded spectrum of CFHQS J142952+544717 in the quasar’s rest frame. The spectrum was unfolded and unabsorbed using the best-fitting model 1 in Table 1, which is shown by the black solid line. The spectral bins are combined to have at least 5σ significance.

CFHQS J142952+544717, discussed in detail in Medvedev et al. (2020), together with the refined X-ray spectrum reported here suggest that the SED’s maximum is located between ~ 10 eV and ~ 1 keV (rest frame), i.e. in the UV-soft X-ray range. Within the accretion disc–corona scenario, this would imply that the luminosity of the Comptonization component is comparable to that of the thermal emission from the disc. Specifically, the corona’s luminosity, L_c , is then at least $\approx 5 \times 10^{46} \text{ erg s}^{-1}$ (as directly measured by *XMM-Newton* between rest-frame 1.4 and 72 keV) and more likely as high as $\sim 10^{47} \text{ erg s}^{-1}$ (if we extrapolate the $\Gamma_x \sim 2.5$ power-law spectrum down to 100 eV and up to ~ 100 keV); whereas the disc’s luminosity, L_d , can be estimated by integrating the optical–UV part of the SED (see Medvedev et al. 2020) to be $\sim 10^{47} \text{ erg s}^{-1}$. The inferred ratio $L_d/L_c \sim 1$ is within the range of typical values for

Seyfert galaxies in the local Universe, $L_d/L_c \sim 1-3$, but lower than the corresponding range, $L_d/L_c \sim 3-6$, for typical, more luminous quasars in the Universe whose combined emission constitutes the bulk of the cosmic X-ray background (Sazonov et al. 2004, 2012). Moreover, many authors (e.g. Lusso et al. 2010) have reported a trend of the SED's optical-to-X-ray (between 2500Å and 2 keV) effective slope increasing with increasing AGN luminosity, which would suggest that the L_d/L_c ratio should be particularly high for such a luminous quasar as CFHQS J142952+544717 in contrast to what is observed.

We thus conclude (cf. Medvedev et al. 2020) that CFHQS J142952+544717 deviates in its SED characteristics from the trends typically observed for quasars. The unusually steep X-ray spectrum and high X-ray/optical luminosity ratio indicate that the accretion disc's corona is probably not responsible for the bulk of the X-ray emission observed from CFHQS J142952+544717.

4.1 X-ray jets

We suggest that the extreme X-ray luminosity of CFHQS J142952+544717 (both the absolute value and the X-ray/optical ratio) is linked with its relativistic jets, the existence of which is evident from the fact that CFHQS J142952+544717 is a radio-loud quasar. Specifically, the observed X-ray emission might be produced by inverse Compton scattering of cosmic microwave background (CMB) photons off relativistic electrons in the jets.

As discussed in Medvedev et al. (2020), according to its multi-wavelength properties (in particular, the fairly steep spectrum and low brightness temperature of the radio emission as well as weak variability in all the observed energy ranges from radio to X-rays), CFHQS J142952+544717 is unlikely to be a blazar, i.e. its jet is not pointing at us. In order to make some crude estimates below, we assume that the jets have a bulk Lorentz factor $\Gamma = 5$ and are oriented at a moderate angle $\cos \alpha \approx 1 - 1/\Gamma$ (i.e. $\alpha \approx 40^\circ$ for $\Gamma = 5$) with respect to our line of sight so that the bulk Doppler factor $\delta = 1/\Gamma(1 - \beta \cos \alpha) \sim 1$ and can be omitted from the consideration.

The typical Lorentz factors, γ , of the electrons that up-scatter CMB photons to the X-ray range can be estimated from the standard relation $E(1+z) \sim (4/3)\Gamma\gamma^2\langle h\nu \rangle$, which takes into account the fact that the incident CMB photons are typically blueshifted by a factor $\sim \Gamma$ due to the relativistic motion of the jet. Here, $\langle h\nu \rangle \approx 2.8kT_{\text{CMB}}(1+z)/h$ is a typical energy of the CMB photons, which can be taken to be equal to the peak energy of the Planck spectrum, $T_{\text{CMB}} = 2.725$ K is the CMB temperature at $z = 0$, E is the observed energy of the up-scattered photons, and $z = 6.18$ is the object's redshift. Given that the X-ray spectrum measured with *XMM-Newton* is a power law with $\alpha_x = 1.5 \pm 0.2$ ($dF_E/dE \propto E^{-\alpha_x}$) between $E_{\text{min}} = 0.2$ keV and $E_{\text{max}} = 10$ keV, we infer that the energy distribution of the underlying population of relativistic electrons extends down to at least $\gamma_{\text{min}} \sim 500/\Gamma \sim 100$ and up to at least $\gamma_{\text{max}} \sim 3000/\Gamma \sim 600$ and its energy distribution ($dN_e/d\gamma \propto \gamma^{-p_x}$) has a slope of $p_x = 2\alpha_x + 1 = 4 \pm 0.4$ ². The cooling time of such electrons due to the inverse Compton scattering of the CMB photons at $z = 6.18$ can be found as:

$$t_{\text{cool}} = \frac{3m_e c^2}{16\sigma_T \sigma_{\text{CMB}}^4 (1+z)^4 \Gamma^2 \gamma} \approx 6 \times 10^6 \left(\frac{\Gamma}{5}\right)^{-2} \gamma^{-1} \text{ yr}, \quad (1)$$

where σ_T is the Thomson cross-section, σ is the Stefan–Boltzmann

² In view of other significant uncertainties in the presented scenario, we ignore here the possible impact of the exact shape of the relativistic Compton scattering kernel on these crude estimates.

constant, and we have taken into account that the CMB energy density is enhanced by a factor of Γ^2 in the comoving frame of the jet (e.g. Ghisellini & Tavecchio 2009). We find that $t_{\text{cool}}(\gamma_{\text{min}}) \sim 3 \times 10^5/\Gamma \sim 6 \times 10^4$ yr and $t_{\text{cool}}(\gamma_{\text{max}}) \sim 5 \times 10^4/\Gamma \sim 10^4$ yr.

The X-ray jet will thus have a size of $\lesssim 20$ kpc (the distance travelled at a speed close to that of light over the cooling time of the lowest-energy X-ray emitting electrons). For viewing angles $\alpha \approx 40^\circ$, the expected angular size of the jet is thus $\lesssim 2$ arcsec.

For comparison, the observed spectrum of the radio emission from CFHQS J142952+544717 between $\nu_{\text{min}} = 120-168$ MHz and $\nu_{\text{max}} = 32$ GHz can be approximately described by a power law with $\alpha_r = 0.7 \pm 0.3$ ($dF_\nu/d\nu \propto \nu^{-\alpha_r}$, see Medvedev et al. 2020; Shao et al. 2020 and references therein), i.e. it is significantly flatter than the X-ray spectrum. The flux density at the lowest available frequency ν_{min} is $S_\nu \approx 10$ mJy (Shimwell et al. 2019). This implies that the synchrotron spectrum peaks at $\nu_p < 120$ MHz and has a maximum intensity $S_p > 10$ mJy. Based on the standard synchrotron self-absorption argument, the required magnetic field $B \sim f(\gamma)^{-5} \theta^4 \nu_p^5 S_p^{-2} (1+z)^{-1}$ (Kellermann & Pauliny-Toth 1981), where $f(\gamma) \sim 8$ is a weak function of γ , θ is the size of the radio source in milliarcseconds, and ν_p and S_p are measured in GHz and Jy, respectively. The size of CFHQS J142952+544717 at the lowest radio frequencies is unknown, but the source has been resolved at 1.6 GHz with the inferred characteristic size ≈ 3 mas (Frey et al. 2011). This corresponds to a physical size of ≈ 20 pc, which is a factor of $\lesssim 10^3$ shorter than the expected size of the X-ray jet (see above). We then find:

$$B \sim 3 \times 10^{-5} \left(\frac{\theta}{3 \text{ mas}}\right)^4 \left(\frac{\nu_p}{100 \text{ MHz}}\right)^5 \left(\frac{10 \text{ mJy}}{S_p}\right)^2 \text{ G}. \quad (2)$$

This implies that the electrons responsible for the synchrotron radio continuum between 120 MHz and 32 GHz have a power-law distribution with a slope of $p_r = 2.4 \pm 0.6$ between $\gamma \sim 3 \times 10^3$ and $\sim 5 \times 10^4$ (for the fiducial parameter values in the equation above). Therefore, the electrons producing the radio emission are more energetic and have a flatter energy distribution than the electrons that presumably produce the X-ray emission via inverse Compton scattering of the CMB photons.

The above consideration suggests the following possible scenario for CFHQS J142952+544717. The quasar has been active for at least a few tens of thousands years, so that high-energy electrons have had enough time to cool down to γ_{min} (see the corresponding estimates above). A power-law distribution of electrons with $p \sim 2.4$ has been constantly supplied to the jets. The observed radio emission is produced via the synchrotron mechanism by freshly generated energetic electrons close to the central source, where there are also sufficiently strong magnetic fields. As the electrons propagate farther away from the central source, they are cooled via inverse Compton scattering of the CMB photons. The observed steep X-ray spectrum reflects the modified population of electrons, which results from the balance between injection and inverse-Compton energy losses of electrons. The theoretically expected difference between the modified and initial slopes of the electron energy distribution $p' - p = 1$ (Kardashev 1962) is consistent, within the measurement uncertainties, with the value inferred here for CFHQS J142952+544717 from the observed slopes of the X-ray and radio spectra: $p_x - p_r = 1.6 \pm 0.7$.

Is this scenario self-consistent? First of all, we should check if inverse Compton scattering of emission from the accretion disc of the central supermassive black hole could cause additional significant energy losses for the electrons in the jets. Assuming that the central source is point-like, we may estimate the radiation energy density at distance r from it in the comoving frame of the relativistic jet as

$U_{\text{QSO}} \sim L_{\text{QSO}}/16\pi\Gamma^2 cr^2$ (e.g. Dermer & Schlickeiser 1993). This should be compared with the energy density of the CMB as seen by the jet, $U_{\text{CMB}} = 4\sigma T_{\text{CMB}}^4 (1+z)^4 \Gamma^2/c$. Taking the bolometric luminosity of the central source to be $L_{\text{QSO}} \sim 2 \times 10^{47} \text{ erg s}^{-1}$ (see above), we infer that the CMB starts to dominate at $\sim 140 \text{ pc}$ from the black hole. The jet propagation time out to this distance is $\sim 500 \text{ yr}$, which is shorter by a factor of ~ 20 than the characteristic cooling time (at this distance) $t_{\text{cool}}(\gamma_{\text{max}}) \sim 10^4 \text{ yr}$ of the highest energy electrons presumably responsible for the observed X-ray radiation (see eq. [1]). This suggests that the quasar’s optical–X-ray radiation probably plays an important role in cooling the electrons in the inner regions of the jets (and leads to the production of gamma-ray emission as a result), but it should not dramatically affect our conclusion that kpc-scale X-ray jets can form in this system.

We should next compare the synchrotron and inverse Compton energy losses. From equation (2), for the quoted fiducial values of the parameters we find that the magnetic energy density within the (radio) jets $U_B = B^2/8\pi \sim 4 \times 10^{-11} \text{ erg cm}^{-3}$ is a factor of $\sim 10^3$ smaller than the CMB energy density in the comoving frame ($U_{\text{CMB}} \sim 3 \times 10^{-8} \text{ erg cm}^{-3}$). This is largely consistent with the observed proportion of the radio and X-ray luminosities of CFHQS J142952+544717=SRGE J142952.1+544716: \sim a few 10^{43} and \sim a few $10^{46} \text{ erg s}^{-1}$, respectively (Medvedev et al. 2020).

We can further estimate the energy density of the radio photons within the jet, based on the luminosity and angular size of the radio source as $U_{\text{radio}} \sim$ a few $10^{-9} \text{ erg s}^{-1}$, which is an order of magnitude smaller than U_{CMB} . Therefore, the synchrotron self-Compton mechanism is probably a minor contributor to the observed X-ray emission.

We thus conclude that the inverse Compton/CMB/jet scenario is a feasible one for explaining the unusual properties of CFHQS J142952+544717. The object may prove to be the most spectacular example so far of an anticipated population (e.g. Ghisellini et al. 2014) of high-redshift quasars with bright X-ray/weak radio jets. So far only a few such objects have been found via direct X-ray/radio imaging (Simionescu et al. 2016; Schwartz et al. 2020). In these objects, at redshifts between 2.5 and 4.7, the inferred jet/quasar luminosity ratio ranges from ~ 1 to ~ 20 per cent. In the case of CFHQS J142952+544717, at $z = 6.18$, we might be dealing with a more extreme case when the jet’s luminosity (and hence its mechanical power) is comparable to that of the accretion disc. As discussed above, the expected size of the X-ray jet in this scenario is $\leq 2 \text{ arcsec}$. Therefore, there is a hope that it could be spatially resolved with the *Chandra X-ray Observatory*, which would be a crucial observation for understanding the nature of high-redshift radio-loud quasars.

ACKNOWLEDGEMENTS

This work is based on observations obtained with *XMM-Newton*, an ESA science mission with instruments and contributions directly funded by ESA Member States and NASA. This work was partially supported by the Russian Science Foundation, project #19-12-00369. We made use of the corner Python module³ for visualizing the posterior probability distributions (Foreman-Mackey 2016). We are grateful to the anonymous referee for their constructive comments and suggestions.

DATA AVAILABILITY

The data used here is publicly available in ESA’s XMM-Newton data archive.

REFERENCES

- Akaike H., 1974, *IEEE Transactions on Automatic Control*, 19, 716
 Arnaud K. A., 1996, in Jacoby G. H., Barnes J., eds, *Astronomical Society of the Pacific Conference Series Vol. 101, Astronomical Data Analysis Software and Systems V*. p. 17, <http://adsabs.harvard.edu/abs/1996ASPC...101...17A>
 Bañados E., et al., 2016, *ApJS*, 227, 11
 Cash W., 1979, *ApJ*, 228, 939
 Dermer C. D., Schlickeiser R., 1993, *ApJ*, 416, 458
 Feigelson E. D., Babu G. J., 2012, *Modern Statistical Methods for Astronomy*
 Foreman-Mackey D., 2016, *The Journal of Open Source Software*, 1, 24
 Frey S., Paragi Z., Gurvits L. I., Gabányi K. É., Cseh D., 2011, *A&A*, 531, L5
 Gabriel C., Rosen S., Webb N., Rodríguez P., Ojero-Pascual E., Perea J. V., 2017, in Lorente N. P. F., Shorridge K., Wayth R., eds, *Astronomical Society of the Pacific Conference Series Vol. 512, Astronomical Data Analysis Software and Systems XXV*. p. 333
 Ghisellini G., Tavecchio F., 2009, *MNRAS*, 397, 985
 Ghisellini G., Celotti A., Tavecchio F., Haardt F., Sbarrao T., 2014, *MNRAS*, 438, 2694
 Goodman J., Weare J., 2010, *Communications in Applied Mathematics and Computational Science*, 5, 65
 HI4PI Collaboration et al., 2016, *A&A*, 594, A116
 Hudelot P., et al., 2012, *VizieR Online Data Catalog*, p. II/317
 Jansen F., et al., 2001, *A&A*, 365, L1
 Kardashev N. S., 1962, *Soviet Ast.*, 6, 317
 Kellermann K. I., Pauliny-Toth I. I. K., 1981, *ARA&A*, 19, 373
 Lusso E., et al., 2010, *A&A*, 512, A34
 Malizia A., Molina M., Bassani L., Stephen J. B., Bazzano A., Ubertini P., Bird A. J., 2014, *ApJ*, 782, L25
 Medvedev P., et al., 2020, *MNRAS*, 497, 1842
 Nanni R., Vignali C., Gilli R., Moretti A., Brandt W. N., 2017, *A&A*, 603, A128
 Ricci C., et al., 2017, *ApJS*, 233, 17
 Sazonov S. Y., Ostriker J. P., Sunyaev R. A., 2004, *MNRAS*, 347, 144
 Sazonov S., et al., 2012, *ApJ*, 757, 181
 Schwartz D. A., et al., 2020, *ApJ*, 904, 57
 Shao Y., Wagg J., Wang R., Carilli C. L., Riechers D. A., Intema H. T., Weiss A., Menten K. M., 2020, *A&A*, 641, A85
 Shemmer O., Brandt W. N., Netzer H., Maiolino R., Kaspi S., 2008, *ApJ*, 682, 81
 Shimwell T. W., et al., 2019, *A&A*, 622, A1
 Simionescu A., et al., 2016, *ApJ*, 816, L15
 Strüder L., et al., 2001, *A&A*, 365, L18
 Turner M. J. L., et al., 2001, *A&A*, 365, L27
 Wang R., et al., 2011, *ApJ*, 739, L34
 Willott C. J., et al., 2010, *AJ*, 139, 906
 Wilms J., Allen A., McCray R., 2000, *ApJ*, 542, 914

This paper has been typeset from a $\text{\TeX}/\text{\LaTeX}$ file prepared by the author.

³ <https://github.com/dfm/corner.py>